Surface roughness and surface-induced resistivity of gold films on mica: influence of roughness modelling

2000 J. Phys.: Condens. Matter 12 2903

(http://iopscience.iop.org/0953-8984/12/13/302)

J. Phys.: Condens. Matter **12** (2000) 2903–2912. Printed in the UK PII: S0953-8984(00)08042-5

Surface roughness and surface-induced resistivity of gold films on mica: influence of roughness modelling

Raúl C Munoz†‖, Guillermo Vidal‡, Germán Kremer§, Luis Moraga§, Claudio Arenas‡ and Andres Concha†

† Departamento de Física, Facultad de Ciencias Físicas y Matemáticas, Universidad de Chile, Blanco Encalada 2008, Casilla 487-3, Santiago, Chile
‡ Departamento de Ingeniería Eléctrica, Facultad de Ciencias Físicas y Matemáticas, Universidad de Chile, Blanco Encalada 2008, Casilla 487-3, Santiago, Chile
§ Departamento de Física, Facultad de Ciencias, Universidad de Chile, Las Palmeras 3425, Santiago, Chile

E-mail: ramunoz@tamarugo.cec.uchile.cl

Received 22 September 1999

Abstract. We report measurements of the temperature dependent resistivity $\rho(T)$ of a gold film 70 nm thick deposited on mica preheated to 300 °C in UHV, performed between 4 K and 300 K, and measurements of the surface topography of the same film performed with a scanning tunnelling microscope (STM). From the roughness measured with the STM we determine the parameters δ (r.m.s. amplitude) and ξ (lateral correlation length) corresponding to a Gaussian and to an exponential representation of the average autocorrelation function (ACF). We use the parameters δ and ξ determined via STM measurements to calculate the quantum reflectivity R, and the temperature dependence of both the bulk resistivity $\rho_0(T)$ and of the increase in resistivity $\Delta\rho(T) = \rho(T) - \rho_0(T)$ induced by electron–surface scattering on this film, according to a modified version of the theory of Sheng, Xing and Wang recently proposed (Munoz *et al* 1999 *J. Phys.: Condens. Matter* **11** L299). The resistivity ρ_0 in the absence of surface scattering predicted for a Gaussian representation of the ACF is systematically smaller than that predicted for an exponential representation of the ACF at all temperatures. The increase in resistivity $\Delta\rho$ induced by electron–surface scattering predicted for a Gaussian representation of the average ACF data is about 25% larger than the increase in resistivity predicted for an exponential representation of the ACF data.

1. Introduction

The effect of electron–surface scattering on the transport properties of thin metallic and semiconducting films is a fundamental problem in solid state physics that remains unsolved, despite over 50 years of research. One of the central questions concerning thin metallic and semiconducting structures is how the surface of the structure affects its electrical transport properties, when one or more of the dimensions characterizing the structure are comparable to or smaller than the mean free path l of the charge carriers, what is known as 'size effects'. The theoretical work concerning size effects focused for many decades on the Fuchs–Sondheimer (FS) model [1, 2], a solution of the Boltzmann transport equation where the effect of the rough surface is incorporated into the boundary conditions that must be satisfied by the electron distribution function, via a specularity parameter R that represents the fraction of electrons $0 \leqslant R \leqslant 1$ that are specularly reflected upon colliding with the rough surface.

‖ Corresponding author.

0953-8984/00/132903+10$30.00

The experimental work related to size effects in thin metal films during many decades relied on the method of: (i) preparing families of samples of the same material but of different thickness under similar conditions of evaporation; (ii) measuring one or more of the transport properties of the different members of the family; (iii) fitting the theoretical models to the thickness dependence of the data, adjusting the parameters provided by the semiclassical theory (specularity parameter R and bulk resistivity ρ_0, among others).

The goal of theoretical research on size effects has been to build a formalism that would permit the prediction of both the reflectivity R characterizing electron–surface scattering and of the increase of resistivity due to size effects from first principles, from the information contained in the surface roughness profile. The development of a many-body quantum transport formalism has led to the formulation of different theories applicable to several special cases. A significant step towards building a formalism applicable to continuous films of arbitrary thickness is the theory of Sheng, Xing and Wang (SXW), that unifies the available quantum transport theories applicable to the different special cases with the classical FS formalism [3]. However, in their treatment SXW modelled the surface roughness by a white-noise surface profile, assuming that the Fourier transform of the height–height autocorrelation function (ACF), that on average characterizes the surface, is a constant independent of the in-plane momentum [3]. This white-noise approximation severely limits the predictive power of the SXW formalism.

We have recently proposed a modified version of SXW theory (mSXW) that permits the calculation of the reflectivity R and of the increase of resistivity attributable to electron–surface scattering, in films in which the average ACF is characterized either by a Gaussian or by an exponential, in terms of the r.m.s. amplitude δ and of the lateral correlation length ξ that describe the average ACF on a nanoscopic scale for either of the two models, Gaussian or exponential, in a continuous film of thickness t [4]. The parameters ξ and δ can be determined independently from measurements of the roughness of the film with a scanning tunnelling microscope (STM). Two of the main conclusions reached in [4] are:

(a) The predictions of mSXW theory and of FS theory *disagree in the case of relatively thick films* (e.g. films having many subbands). For $t/l > 1$, the FS model overestimates the effect of electron–surface scattering by an amount that increases with increasing l for a fixed t, due to the fact that the angular dependence of the quantum reflectivity R is completely ignored in the FS theory.
(b) The predictions of mSXW theory *are model dependent*. The values of σ/σ_0 (σ: film conductivity, σ_0: conductivity in the bulk) predicted by theory for a Gaussian representation of the ACF data are different from the values predicted for an exponential representation of *the same data*.

Nevertheless, there are certain interesting questions that arise from the mSXW formalism, that we did not address in [4] because of limitations of space imposed by the format of a short communication:

(i) Electrons are scattered by the *individual* corrugations they find when approaching the rough surface. However, the mSXW theory provides answers that depend on the parameters δ and ξ that characterize the *average* ACF. The relationship between *individual* corrugations and *average* surface roughness needs to be elucidated.
(ii) Why is the reflectivity predicted by mSXW theory (figure 2 [4]) such that it approaches zero for a certain angle?
(iii) How can the mSXW theory be used to *calculate* the bulk resistivity $\rho_0(T) = 1/\sigma_0(T)$ from the measured film resistivity $\rho(T) = 1/\sigma(T)$ and from the surface roughness measured with the STM, *without using adjustable parameters*? Are the values predicted by theory for the bulk resistivity $\rho_0(T)$ and for the increase in resistivity $\Delta\rho(T) = \rho(T) - \rho_0(T)$

induced by electron–surface scattering, *also model dependent*? Do the predictions for $\rho_0(T)$ and for $\Delta\rho(T)$ also depend on whether the ACF data is represented by a Gaussian or by an exponential? In this paper we address these questions.

In this work we report measurements of the temperature dependent resistivity $\rho(T)$ of a gold film 70 nm thick deposited on mica preheated to 300 °C in UHV, performed between 4 K and 300 K, and measurements of the surface topography of the *same* film performed with a STM. From the roughness measured with the STM we determine the parameters δ and ξ corresponding to a Gaussian and to an exponential representation of the average ACF data. We use, for the first time, the parameters δ and ξ determined via STM measurements to calculate the quantum reflectivity R, and the temperature dependence of both the bulk resistivity $\rho_0(T)$ and of the increase in resistivity $\Delta\rho(T)$ induced by electron–surface scattering on this film, according to mSXW theory. We compare the results obtained analysing the data using the mSXW theory for both a Gaussian and an exponential representation of the average ACF data. We assess the influence of roughness modelling as well as the validity of the assumptions underlying the FS model in the case of relatively thick metal films having many subbands.

2. Theory

Summarizing results already published, the many-body SXW quantum theory leads to a reformulation of the FS model, that includes the effects of surface scattering via a reflectivity parameter R that can be calculated from

$$R(k_\parallel) = \left(\frac{1 - k_z Q(k_\parallel)}{1 + k_z Q(k_\parallel)}\right)^2 \tag{1}$$

which is equation (7) in [3], where $Q(k_\parallel)$ represents the dissipative part of the self-energy of the electron gas due to electron–surface scattering; with $k_z^2 = k_F^2 - k_\parallel^2$, where k_F stands for the Fermi momentum, $k_\parallel = (k_x, k_y)$ represents the in-plane momentum. The ratio of the film conductivity σ to bulk conductivity σ_0 may be computed in terms of the reflectivity R

$$1 - \frac{\sigma}{\sigma_0} = \frac{3}{2}\frac{l}{t}\frac{1}{X_0 N_c}\sum_{n=1}^{N_c} u_n(1 - u_n^2)\frac{(1 - R(u_n))(1 - E_d(u_n))}{1 - R(u_n)E_d(u_n)} \tag{2}$$

where t is the film thickness, l the carrier mean free path *in the absence of surface scattering*, $u_n = q_n/k_F = \cos\theta_n = n\pi/tk_F$, $X_c = tk_F/\pi$, $N_c = \mathrm{int}(X_c)$ where $\mathrm{int}(M)$ stands for the integer part of M, $X_0 = \frac{3}{2}[1 - \frac{1}{3}(N_c/X_c)^2(1+1/N_c)(1+1/2N_c)]$ and $E_d(u_n) = \exp[-t/(u_n l)]$, which corresponds to equation (11) of [3]. As shown by SXW, this result contains the answers that are already known in the following cases: (a) in the thick–rough film limit where quantum effects can be neglected and bulk scattering dominates over surface scattering, equation (2) reproduces the classical FS result [1, 3]; (b) in the limit where surface and bulk scattering are comparable, equation (2) reproduces the result of Trivedi and Ashcroft [3, 5]; (c) in the limit of ultrathin films where surface scattering is expected to dominate over bulk scattering, equation (2) reproduces the result of Fishman and Calecki [3, 6].

Following SXW, we calculated the self energy $Q(k_\parallel)$ when the average ACF that characterizes the surface is described by a Gaussian $f(x, y) = \delta^2 \exp[-(x^2+y^2)/\xi^2]$, or by an exponential $f(x, y) = \delta^2 \exp[-\sqrt{x^2 + y^2}/\xi]$. The result in the case of a Gaussian ACF is [4]

$$Q(k_\parallel) = \frac{\xi^2\delta^2}{2t}\pi \exp\left[-\frac{\xi^2}{4}\left(k_\parallel^2 + k_F^2\right)\right]\sum_{n=1}^{N_c}\left(\frac{n\pi}{t}\right)^2 \exp\left[\left(\frac{n\pi}{t}\right)^2\frac{\xi^2}{4}\right] \times I_0\left(\frac{\xi^2}{2}k_\parallel\sqrt{k_F^2 - \left(\frac{n\pi}{t}\right)^2}\right) \tag{3}$$

where $I_0(x)$ stands for the modified Bessel function of order zero [7]. In the case of an exponential ACF we obtain [4]

$$Q(k_\parallel) = \frac{2\xi^2\delta^2}{t}\sum_{n=1}^{N_c}\left(\frac{n\pi}{t}\right)^2 \frac{E[r^2(k_\parallel, q_n)]}{[1+\xi^2(k_\parallel - q_n)^2]\sqrt{1+\xi^2(k_\parallel - q_n)^2}} \tag{4}$$

with

$$r^2(k_\parallel - q_n) = \frac{4\xi^2 k_\parallel q_n}{1+\xi^2(k_\parallel + q_n)^2}$$

where $E(r^2)$ stands for the elliptic integral of second kind [8].

3. Experiment

We performed some preparatory experiments to select the conditions of evaporation. The temperature of the substrate, 300 °C, the speed of evaporation, 6 nm min^{-1}, and the thickness of the film, 70 nm, were chosen such as to produce a continuous film where the influence of grain-boundary scattering would be minimized, for grain-boundary scattering could influence the resistivity of the film but is *not included in the SXW theory*. The gold films were prepared by thermal evaporation of 2 mm diameter, 99.99% pure gold wire (Matkemi) from a W basket onto 20 mm × 10 mm × 0.15 mm Muscovite ruby mica slides (Goodfellow). The mica was freshly cleaved before evaporation. The stainless steel evaporator was baked for many hours after loading the mica and the gold wire until reaching a pressure in the range of 10^{-10} mbar. The thickness of the gold films was monitored during evaporation with a quartz crystal oscillator that was calibrated with a profilometer (Tencor). To avoid scratching the surface, the thickness was measured with the profilometer *after* the surface roughness and resistivity of the samples had been measured. During evaporation the pressure was in the range of 10^{-9} mbar.

During the preparatory experiments designed to select the conditions of evaporation, the samples were examined using x-ray diffraction; the crystallographic structure of the films and of the mica was determined using a Siemens D-5000 x-ray diffractometer. The samples were also examined using a scanning electron microscope (SEM). The samples were kept under moderate vacuum in a dessicator between the different experimental steps (measurements of the roughness with the STM, x-ray measurements, SEM measurements, resistivity measurements, determination of the thickness with the profilometer).

The surface topography was measured with the STM running in air in the constant-current mode using W tips. STM measurements were performed with a commercial Omicron instrument, using tungsten tips 0.25 mm in diameter freshly etched in a 0.8 M NaOH solution. All images had 256 × 256 pixels. We verified that the images did not depend on the gap voltage or on the tunnelling current. Before imaging the gold samples, we verified that the freshly prepared W tips produced neat images of C atoms running on HOPG. Tips that did not produce neat images of C atoms on HOPG were discarded.

We paid particular attention to searching with the STM for direct experimental evidence of barriers existing between adjacent grains. For this purpose we imaged with the STM the valleys that are left after the grains coalesce to form the film. The bottom of these valleys look fairly smooth within an atomic scale. We did not find any sharp changes in the STM signal recorded on these valleys on an atomic scale, that might indicate the presence of a barrier between adjacent grains.

Conductivity measurements were performed using the four-probe method, running a current of 100 μA pp at 160 Hz, using SRS 830 lock-in amplifiers from Stanford Research. Data acquisition was computer controlled; the voltage drop across the sample was averaged

over 100 data points, the relative error in the voltage reading is estimated at two parts in 10 000. The sample was mounted on a Cu block located in the variable temperature insert of the Dewar of a 9 T (Janis) superconducting magnet. The temperature of the Cu block was maintained within ± 0.1 K between 4 K and 300 K.

4. Results

A short report has been published containing the measurements of the surface roughness. The quantity measured with the STM is the function $h(a_{\|})$ defined by equation (3) of [4]. The data representing the peak at the origin of the average ACF displayed in figure 1 of [4] was fitted using a Gaussian $f(x, y) = \delta^2 \exp[-(x^2 + y^2)/\xi^2]$ and an exponential $f(x, y) = \delta^2 \exp[-\sqrt{x^2 + y^2}/\xi]$, employing a least squares fit procedure, choosing 6×6, 8×8, 10×10 and 12×12 pixels near the origin. The values obtained for δ and ξ as well as the corresponding values for χ^2 are listed in table 1. The values obtained for δ and ξ are consistent with the atomic resolution exhibited by the tip of the STM when running on HOPG prior to measuring the gold sample. Consequently, the rounding off that could be expected on the images recorded with the STM due to the finite radius of curvature of the tip, does not seem to play a significant role. A glance at table 1 reveals that both the Gaussian and the exponential provide a good fit (as indicated by the low values of χ^2) to the experimental ACF data, although the fitting by an exponential seems consistently better than the fitting by a Gaussian, for the values obtained for χ^2 are at least a factor of three lower. The r.m.s. amplitude δ for the exponential ACF turns out to be about 30% larger than the value corresponding to the Gaussian ACF.

4.1. Average ACF

It seems appropriate to point out that although electrons are scattered by the individual corrugations they find when approaching the rough surface, in the theoretical treatment of electron–surface scattering usually an average is performed over all corrugations found in the surface. Consequently, the final answer depends on some average property of the surface, rather than on the individual corrugations. In quantum theories of electron–surface scattering, the *average corrugations* of a randomly rough surface are often assumed to be *isotropic* [3, 5, 6, 9, 10]. This means that, if $f(x, y)$ denotes the ACF computed from the surface roughness profile according to equation (3) of [4], it is expected that after averaging over the surface, $f(x, y) = f(\sqrt{x^2 + y^2})$. However, we found that the ACFs computed from each individual image recorded on this film may differ by as much as one order of magnitude or more, and may exhibit quite different structures such as bumps and undulations away from

Table 1. Parameters characterizing the ACF data. δ = r.m.s. amplitude; ξ = lateral correlation length. χ^2 = chi square, parameter characterizing the goodness of the fit.

	Exponential			Gaussian		
	δ	ξ	χ^2	δ	ξ	χ^2
6×6	0.746	0.198	0.137	0.539	0.344	0.461
8×8	0.687	0.231	0.498	0.494	0.401	2.21
10×10	0.633	0.271	0.821	0.448	0.489	3.78
12×12	0.602	0.299	1.510	0.422	0.549	7.81
$\langle x \rangle$	0.667	0.250		0.476	0.446	

the origin along x or along y, where (x, y) stand for the (fast, slow) scan direction of the STM, respectively. Nevertheless, the features away from the origin add up to nearly zero upon averaging the ACFs corresponding to each of the STM images, leaving essentially a sharp peak at the origin plus some noise. The ACFs computed from individual images recorded on this film are certainly *not isotropic*; it takes a number of the order of 20 images (or larger), recorded at *random* locations of the sample on a scale of 20 nm × 20 nm, to obtain *an average ACF that is very nearly isotropic*.

4.2. Angular dependence of the quantum reflectivity

The reflectivity R calculated according to the mSXW formalism, using both the Gaussian and exponential models, is shown in figure 1. The reflectivity R is not a constant as function of the angle θ between the momentum of the incoming electron and the normal to the surface. On the contrary, R is approximately zero for a certain angle, the value of which is model dependent. Why the reflectivity approaches zero for a certain angle may be understood in terms of the white-noise model used by SXW. If Q_0 is the momentum-independent self-energy of the electron gas in the lowest order within the white-noise approximation, then the reflectivity is given by $R[f, \cos(\theta)] = [(1 - f\cos(\theta))/(1 + f\cos(\theta))]^2$ [3]. The dimensionless parameter $f = k_F Q_0$ is proportional to the 'strength' of the delta function describing the ACF in (x, y) space—the constant that multiplies the delta function. Regarding the mathematical representation of the ACF data, f is expected to depend roughly on δ^2 the square of the amplitude of the Gaussian or the exponential.

If the surface profile is such that $f > 1$, then the white-noise reflectivity will approach zero for an angle θ_0 given approximately by $\cos\theta_0 = 1/f$. For the film reported here, with the average ACF displayed in figure 1 of [4] described by a Gaussian with $\delta = 0.476$ nm and $\xi = 0.446$ nm, the reflectivity approaches zero for $\cos\theta_0 = 0.1224$. If the average ACF is modelled by an exponential with $\delta = 0.667$ nm and $\xi = 0.250$ nm, then the reflectivity approaches zero for $\cos\theta_0 = 0.077\,89$. The corresponding white-noise dimensionless parameter is $f = 1/\cos(\theta_0) = 8.17$ for the Gaussian, and $f = 1/\cos(\theta_0) = 12.8$ for the exponential representation of the ACF. The reflectivity approaches zero for a smaller angle in the case of the exponential ACF, because the amplitude δ turns out to be larger for this model than for the Gaussian ACF. The white-noise reflectivities corresponding to the Gaussian and exponential representations of the ACF are plotted in figure 1.

4.3. Electron–surface scattering and bulk resistivity

It seems convenient to point out that the predictions of mSXW theory, as well as those of the classical FS theory, both involve the parameters σ_0 and l that characterize the bulk—the conductivity and mean free path that would be measured *in the absence of surface scattering* [1–3], which therefore correspond to a *film having the same concentration of impurities/defects as the thin film, but thick enough such that the effect of electron–surface scattering can be neglected. Neither of these parameters is known a priori*, hence the tendency that prevailed for many decades, to fit conductivity data on a family of samples of different thickness—prepared under similar conditions of evaporation—using as adjustable parameters a constant reflectivity R and the bulk resistivity ρ_0 assumed common to all members of the family. The availability of a quantum theory that predicts R and σ/σ_0 using solely as input the information contained in the surface roughness profile characterizing the sample allows, for the first time, a direct estimation of $\rho_0(T)$ and of the change in resistivity $\Delta\rho(T)$ attributable to electron–surface

scattering. To proceed with such estimations we need to determine l. This can be accomplished by means of an iterative process.

As a first approximation, $l(T)$ corresponding to each temperature can be calculated from $l_1(T) = \sigma(T)mv_F/(nq^2)$, where $\sigma(T)$ is the conductivity of the 70 nm thick film measured at temperature T, m is the electron mass, v_F is the Fermi velocity, n the electron density and q the electron charge. This value is used to compute a first estimation of $[\sigma(T)/\sigma_0(T)]_1$, using $l = l_1$, equation (2) and the parameters δ and ξ determined from the STM measurements. A corrected value for l can then be computed from $l_2 = l_1[\sigma_0(T)/\sigma(T)]_1$, and a new value of $[\sigma(T)/\sigma_0(T)]_2$ can be calculated using $l = l_2$, equation (2) and the parameters δ and ξ. This process is repeated until the values of $[\sigma(T)/\sigma_0(T)]_j$ and $[\sigma(T)/\sigma_0(T)]_{j+1}$ between two successive iterations j and $j + 1$ do not differ by more than 0.01%. We found that four iterations are sufficient to satisfy this criterion. The measured film resistivity $\rho(T)$, as well as the bulk resistivity $\rho_0(T)$ calculated using this iterative procedure, assuming a Gaussian and an exponential ACF, are plotted in figure 2(a). In figure 2(b) we display the temperature dependence of the increase of resistivity $\Delta\rho(T)$ induced by electron–surface scattering calculated for each of the two representations of the ACF, Gaussian and exponential.

The results shown in figure 2(a) indicate that in this thick gold film, the resistivity decreases by roughly a factor of four between 4 K and 300 K, and so does the bulk resistivity ρ_0. A new and interesting result is that $\rho_0(T)$ *turns out to be model dependent*: $\rho_0(T)$ for a Gaussian ACF seems systematically smaller than that for an exponential representation of the ACF. The results displayed in figure 2(b) indicate that the increase in resistivity $\Delta\rho$ induced by electron–surface scattering, besides being model dependent, is perhaps also weakly temperature dependent; $\Delta\rho$

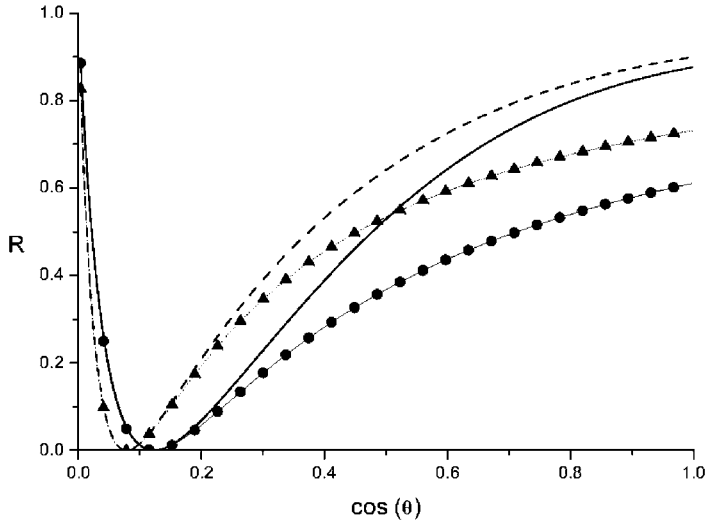

Figure 1. Reflectivity R characterizing electron–surface scattering on a gold film 70 nm thick predicted by the mSXW theory. Solid line: R corresponding to a film in which the average ACF is described by $f(x, y) = \delta^2 \exp[-(x^2 + y^2)/\xi^2]$, with $\delta = 0.476$ nm, $\xi = 0.446$ nm, calculated from equations (1) and (3), plotted as a function of $\cos(\theta)$. θ represents the angle of incidence between the momentum of the incoming electron and the normal to the surface. Circles/solid line: white-noise reflectivity R corresponding to $f = 8.17$. Broken line: reflectivity R corresponding to a film in which the average ACF is described by $f(x, y) = \delta^2 \exp[-\sqrt{x^2 + y^2}/\xi]$, with $\delta = 0.667$ nm, $\xi = 0.250$ nm, calculated from equations (1) and (4). Triangles/broken line: white-noise reflectivity R corresponding to $f = 12.8$.

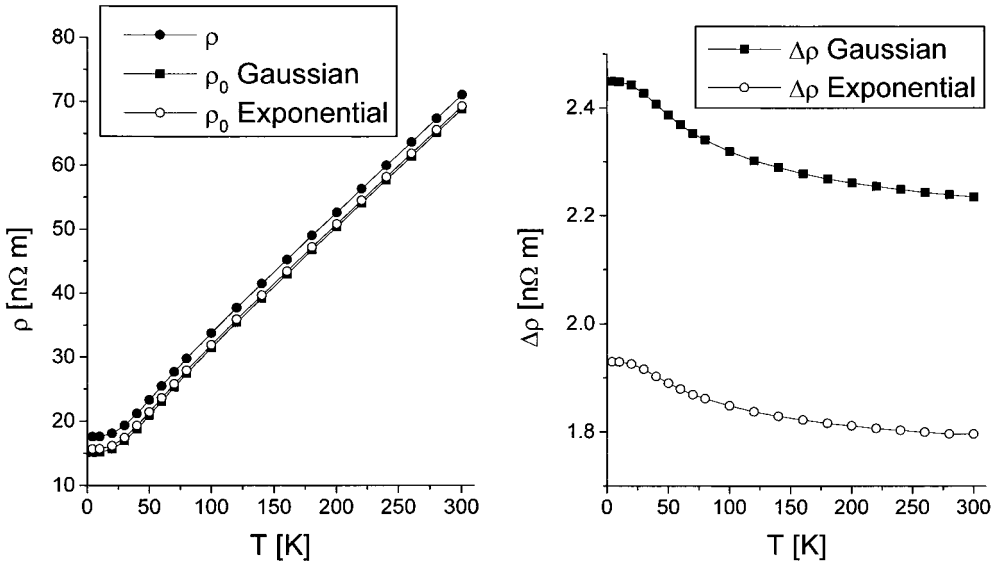

(a) (b)

Figure 2. (a) Resistivity plotted as a function of temperature. Filled circles/solid line: resistivity measured on a 70 nm thick gold film. Open circles/solid dotted line: bulk resistivity $\rho_0(T)$ corresponding to the 70 nm thick film, calculated using mSXW theory and an ACF described by $f(x, y) = \delta^2 \exp[-\sqrt{x^2 + y^2}/\xi]$, with $\delta = 0.667$ nm, $\xi = 0.250$ nm. Filled squares/solid line: bulk resistivity $\rho_0(T)$ corresponding to the 70 nm thick film, calculated using mSXW theory and an ACF described by $f(x, y) = \delta^2 \exp[-(x^2 + y^2)/\xi^2]$, with $\delta = 0.476$ nm, $\xi = 0.446$ nm. (b) Temperature dependence of the increase of resistivity $\Delta\rho(T) = \rho(T) - \rho_0(T)$ induced by electron–surface scattering, calculated according to the mSXW theory, on a 70 nm thick gold film. Squares/solid line: $\Delta\rho(T)$ calculated using mSXW theory and an ACF described by $f(x, y) = \delta^2 \exp[-(x^2 + y^2)/\xi^2]$, with $\delta = 0.476$ nm, $\xi = 0.446$ nm. Circles/solid line: $\Delta\rho(T)$ calculated using mSXW theory and an ACF described by $f(x, y) = \delta^2 \exp[-\sqrt{x^2 + y^2}/\xi]$, with $\delta = 0.667$ nm, $\xi = 0.250$ nm.

predicted for a Gaussian ACF is systematically larger (about 25% larger) than that predicted for an exponential representation of the ACF at all temperatures.

5. Discussion

The data displayed in figure 2(a) indicate that the resistivity of our 70 nm film at 300 K is about three times larger than the intrinsic resistivity due to electron–phonon scattering of crystalline gold at 300 K, $\rho_I(300\ \text{K}) = 22.49\ \text{n}\Omega\ \text{m}$ [11]. Consequently, in spite of the purity of 99.99% of the starting material, there are enough impurities present in the sample that contribute significantly to the resistivity of the film. The resistivity ratio $\text{RR} = \rho(300\ \text{K})/\rho(4\ \text{K}) \approx 4$ in our 70 nm film is comparable to $\text{RR} \approx 6$ reported by Sambles, Elsom and Jarvis (SEJ) in a gold film 80 nm thick thermally evaporated under a pressure of *ca* 10^{-4} Pa onto a mica substrate under conditions of evaporation (substrate preheated to 280 °C, speed of evaporation 5 nm min^{-1}) which are almost identical to ours (substrate preheated to 300 °C, speed of evaporation 6 nm min^{-1}), except for the fact that SEJ used gold 99.9999% pure [12]. The main difference between the resistivity data of the SEJ-80 nm film and the resistivity data of our 70 nm film is that the SEJ-80 nm film exhibits a resistivity at 300 K which is some 20% larger than $\rho_1(300\ \text{K})$, instead of almost three times larger. We attribute this enhanced resistivity,

due to impurities in our sample, to the fact that we used, as starting material, gold which is two orders of magnitude less pure than the gold used by SEJ. With the substrate heated to 280 or 300 °C, it would seem that there are enough impurities migrating from the mica into the film to result in a small but non-negligible contribution to the resistivity of the film arising from impurities in the SEJ-80 nm film *in spite of the stated purity of 99.9999%*, and a contribution due to impurities in our 70 nm film which is *larger* than the intrinsic resistivity $\rho_I(300\ \mathrm{K})$.

To minimize the effect of the roughness of the substrate, we chose mice, a crystalline, insulating, cleavable material that nearly matches the lattice constant of gold. As discussed in [4], the roughness of the mica consists of some cleavage steps which are rather infrequent over a scale of distances $L \leqslant 10$ nm probed by the electrons. Consequently, electron–surface scattering taking place at the gold–mica interface can be safely neglected.

Having selected mica as a substrate, we selected the conditions of evaporation during the preparatory experiments, in order to produce a continuous film where the influence of grain-boundary scattering would be minimized. This meant heating the mica substrate to 300 °C. During the exploratory experiments designed to select the conditions of evaporation, *before* undertaking the laborious task of measuring the average ACF of the film with the STM, the morphology of the samples was monitored via x-ray diffraction and SEM images of the films. The x-ray diffraction spectra indicated that the mica substrate is, indeed, crystalline, and that the gold films are also crystalline, with direction $\langle 111 \rangle$ growing perpendicular to the mica substrate, in agreement with the observations reported in [12]. The SEM images we obtained are also quite similar to images already published (figures 1(c) and 1(d) of [12]), indicating that the typical lateral dimensions of the grains that coalesced to form the film are in the range of several hundred nm. These grains are characterized by lateral dimensions which are about one order of magnitude larger than the grains of gold films deposited on substrates of polished Pyrex, silicon dioxide and silicon nitride at room temperature reported in figure 4(a) of [13].

In our 70 nm film the mean free path l is about 52 nm at temperatures below 10 K and it is smaller at higher temperatures. Therefore the electron undergoes many collisions with impurities/phonons or with the upper/lower surfaces of the film, before it encounters the boundary of a grain. The price paid for using a mica substrate and for heating the mica in order to obtain grains with lateral dimensions that are about one order of magnitude larger than the thickness of the film—such as to warrant that the resistivity of the film is dominated either by impurity/phonon scattering or by electron–surface scattering at the upper/lower surfaces of the film, *and not by grain boundary scattering*—is probably the diffusion of impurities from the mica into the sample, impurities that exhibit a low vapour pressure.

This is in contrast with the resistivity of gold films deposited on substrates of polished Pyrex, silicon dioxide and silicon nitride at room temperature [13]. In films of comparable thickness deposited on these substrates using gold 99.95% pure, the main contribution to the resistivity of the film arising from electron–surface scattering seems dominated by grain-boundary scattering as a consequence of the substrate being at *room temperature during evaporation*, which results in *non-epitaxial films* made up of grains of small lateral dimensions, comparable to the film thickness, about 30 nm (figure 4(a) of [13]). This interpretation of the resistivity data is confirmed by a significant *reduction in the resistivity* of the films measured at 295 K reported in figure 1 of [13] *after heat treating the samples*, that correlates with a *drastic increase in the grain size* detected by transmission electron microscopy (TEM) in the heat-treated samples (figure 4(b) in [13]).

Concerning the influence of roughness modelling, the results reported suggest that *the parameters that control electron–surface scattering in continuous gold films of arbitrary thickness are the r.m.s. amplitude δ and the lateral correlation length ξ that describe the average ACF characterizing the surface of the sample on a nanoscopic scale, independently of*

which model is used to represent the ACF data, in agreement with the accepted view regarding the conductivity of ultrathin films [6, 9, 10]. The quantum reflectivity R is not a constant but depends on the angle of incidence between the momentum of the incoming electrons and the normal to the surface. It turns out that *R depends explicitly on the film thickness t as well as on the roughness of the surface*, because the self-energy of the electron gas (equations (3) and (4)) does depend on t, as well as on ξ and δ. The microscopic description provided by the mSXW theory casts doubts on the validity of one of the central assumptions that has been used to analyse conductivity data for many decades—the assumption that the reflectivity characterizing electron–surface scattering on a family of metal films of different thickness, prepared under similar conditions of evaporation, *is the same for all members of the family*.

The results presented serve to outline a procedure to analyse size-effect data that departs sharply from the parameter fitting of resistivity data that has been employed for decades. *The new procedure outlined in this work permits the calculation of size effects from first principles—without free parameters*—using as input the information contained in the average height–height ACF that characterizes the surface of the sample on a nanometric scale: the r.m.s. amplitude and the lateral correlation length. As shown here, such information is now accessible to direct, independent experimental determination thanks to the invention of the STM.

Acknowledgments

RM, GK and LM gratefully acknowledge funding by Fondo Nacional de Ciencia y Tecnologia FONDECYT under contract 1960914, by Fundacion ANDES under Contract C-12776 and by Universidad de Chile, Departamento de Investigación y Desarrollo, under contract EDID99/008.

References

[1] Sondheimer E H 1952 *Adv. Phys.* **1** 1
[2] Sambles J R 1983 *Thin Solid Films* **106** 321
[3] Sheng L, Xing D Y and Wang Z D 1995 *Phys. Rev.* B **51** 7325
[4] Munoz R C, Vidal G, Kremer G, Moraga L and Arenas C 1999 *J. Phys.: Condens. Matter* **11** L299
[5] Trivedi N and Aschroft N W 1988 *Phys. Rev.* B **38** 12 298
[6] Fishman G and Calecki D 1989 *Phys. Rev. Lett.* **62** 130
[7] Abramowitz M and Stegun I A (ed) 1964 *Handbook of Mathematical Functions (NBS, Applied Mathematics Series vol 55)* (Washington, DC: National Bureau of Standards)
[8] Gradshteyn I S and Ryzhik I M 1980 *Table of Integral, Series and Products* (New York: Academic)
[9] Fishman G and Calecki D 1991 *Phys. Rev.* B **43** 1158
[10] Calecki D and Fishman G 1990 *Surf. Sci.* **229** 110
[11] Matula R A 1979 *J. Phys. Chem. Data* **8** 1147
[12] Sambles J R, Elsom K C and Jarvis D J 1982 *Phil. Trans. R. Soc.* A **304** 365
[13] Van Attekum P M Th M, Woerlee P H, Verkade G C and Hoeben A A M 1984 *Phys. Rev.* B **29** 645